Supporting Information

ZIF-67 Nanoarrays Derived Pd Hybrid Catalyst with Improved Mass Activity and Current Efficiency for Electrocatalytic Reductive Dechlorination of 2,4-Dichlorophenol

Yingxue Yu,† Wenyan Luo,† Qing Gao, Chengyun Wang, Xinyao Li, Honghua Xie and Rui Xiang*

†: These authors contribute equally to this article.
*: College of Chemistry and Chemical Engineering, Chongqing University of Science &Technology, Chongqing, 401331, China. E-mail: 2019045@cqust.edu.cn

1. Equations used for assessing the ERD performance

The EHDC efficiency of 2,4-DCP was calculated by Equation:

$$\alpha = \frac{C_0 - C}{C_0} \times 100\%$$

where α represents the removal rate of 2,4-DCP, C_0 represents the initial concentration of 2,4-DCP, and C represents the concentration at different reaction time t (min) of 2,4-DCP.

Pseudo-first-order kinetics model is used to describe the EHDC reaction, and was calculated by Equation:

$$-ln(C/C_0) = k_{obs} \times t$$

where, K_{obs} (min^{-1}) is the observed rate constants, which is obtained from a linear regression of the lnC/C_0 versus t.

The mass activity (MA, min^{-1} g_{Pd}^{-1}) was estimated by Equation:

$$MA = \frac{k_{obs}}{M_{Pd}}$$

where, k_{obs} is the observed rate constants, M_{Pd} is the mass loading of Pd determined by ICP-OES.

Dechlorination current efficiency (CE%) is calculated by Equation:

$$CE(\%) = \frac{(n_1 \Delta C_p + n_2(\Delta C_{o-cp} + \Delta C_{p-cp})) \times FV}{\int_{t=0}^{t=t} Idt} \times 100\%$$

In the equation, n_1 and n_2 are the number of electron transfers with 2,4-DCP to produce each molecule of P (n_1 = 4) and CP (n_2 = 2), respectively. F is the Faraday constant (96500 C/mol), I is the operating current (A), V is the volume of the reaction electrolyte (70 mL), and t is the reaction time (min).

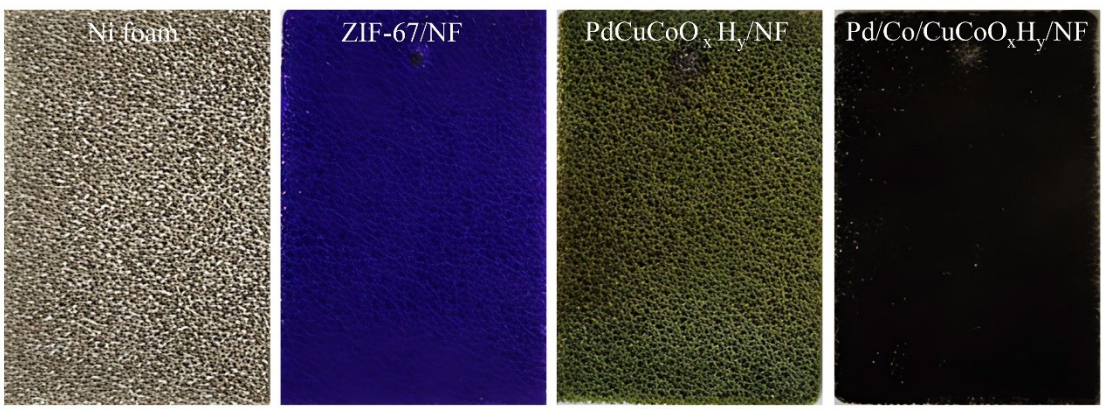

Figure S1. Digital graphs of bare Ni foam, ZIF-67/NF, $PdCuCoO_xH_y$/NF and Pd/Co/$CuCoO_xH_y$/NF.

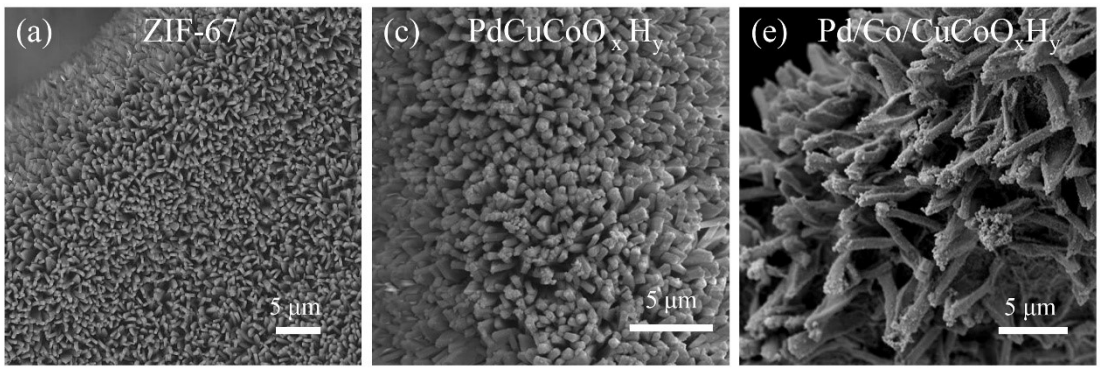

Figure S2, SEM images of ZIF-67 nanoarrays (a), $PdCuCoO_xH_y$ nanoarrays (b) and

Pd/Co/CuCo$O_x$$H_y$/NF nanoarrays (c).

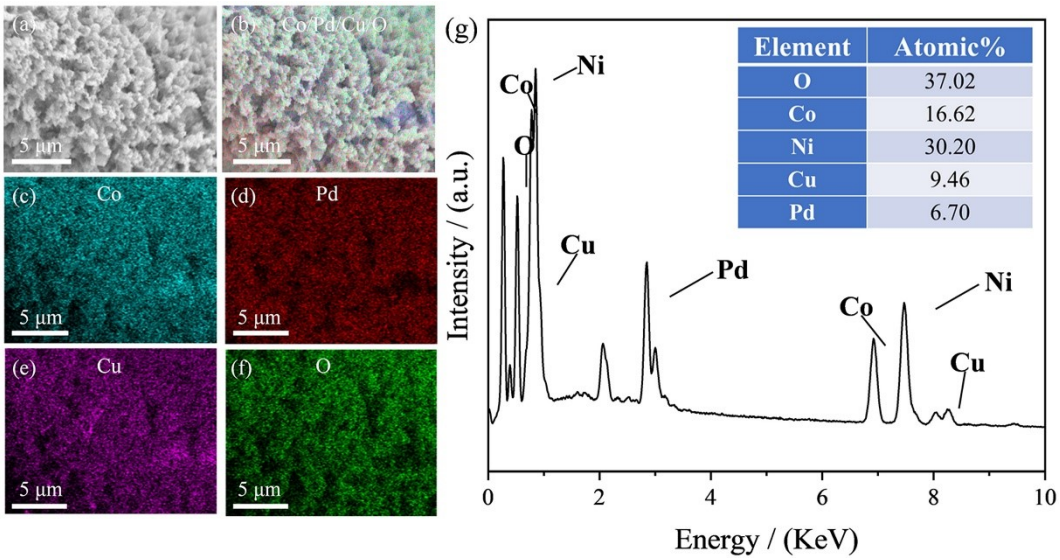

Figure S3. EDS mapping images of Pd/Co/$CuCoO_xH_y$/NF (a-f) and related EDS spectra curve (g).

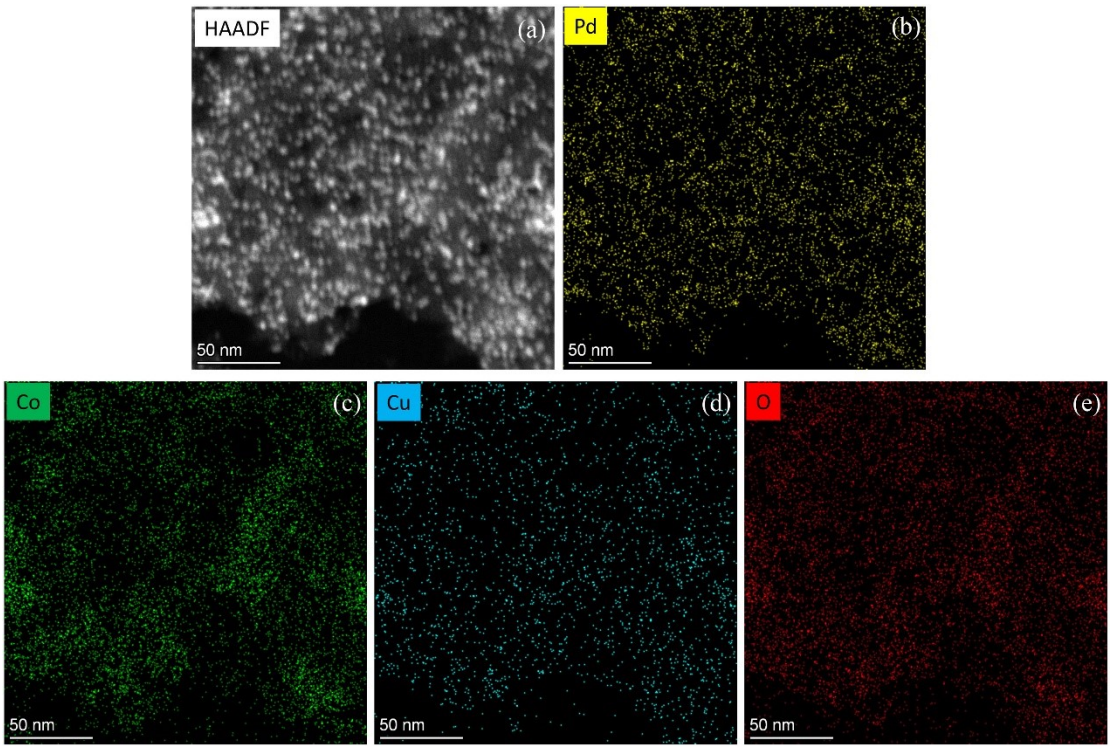

Figure S4. HAADF-STEM image (a) and the corresponding elemental mapping images of Pd (b), Co (c), Cu (d) and O (e) in Pd/Co/$CuCoO_xH_y$/NF.

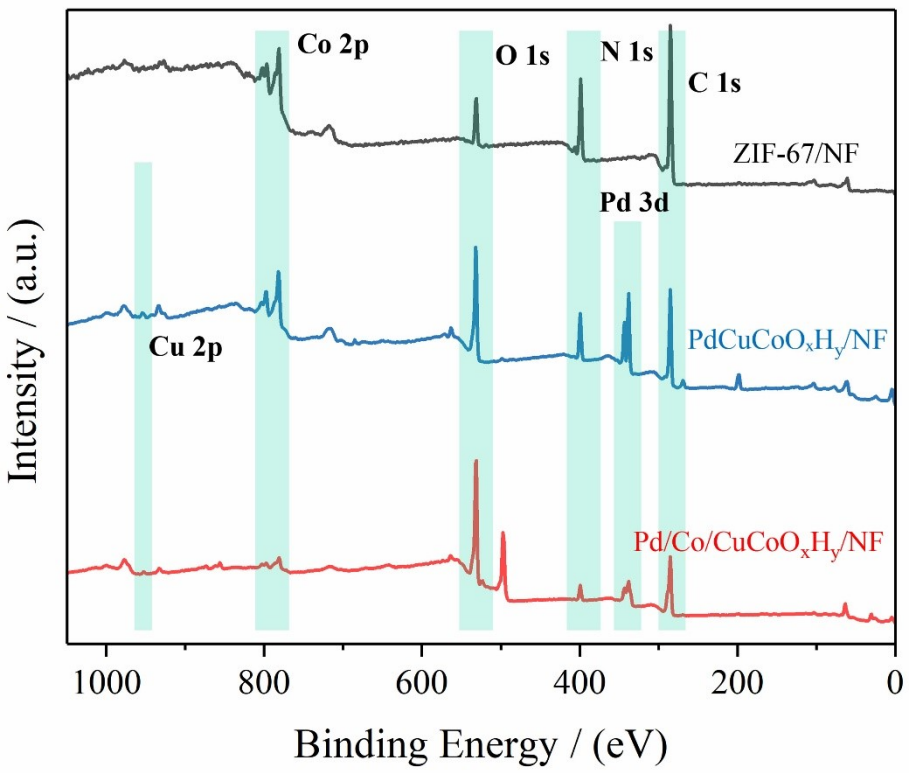

Figure S5. Survey XPS spectra of ZIF-67/NF (black line), PdCuCoO$_x$H$_y$/NF (blue line) and Pd/Co/CuCoO$_x$H$_y$/NF (red line).

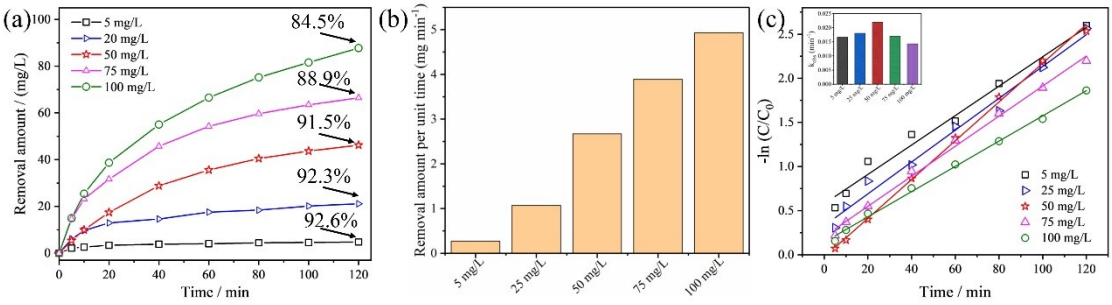

Figure S6. (a) 2, 4-DCP degradation curves catalyzed by Pd/Co/$CuCoO_xH_y$/NF with different initial 2, 4-DCP concentrations. (b) removal amount of 2, 4-DCP per unit time measured with different initial concentrations. (b) Pseudo-first-order reaction kinetics fitting.

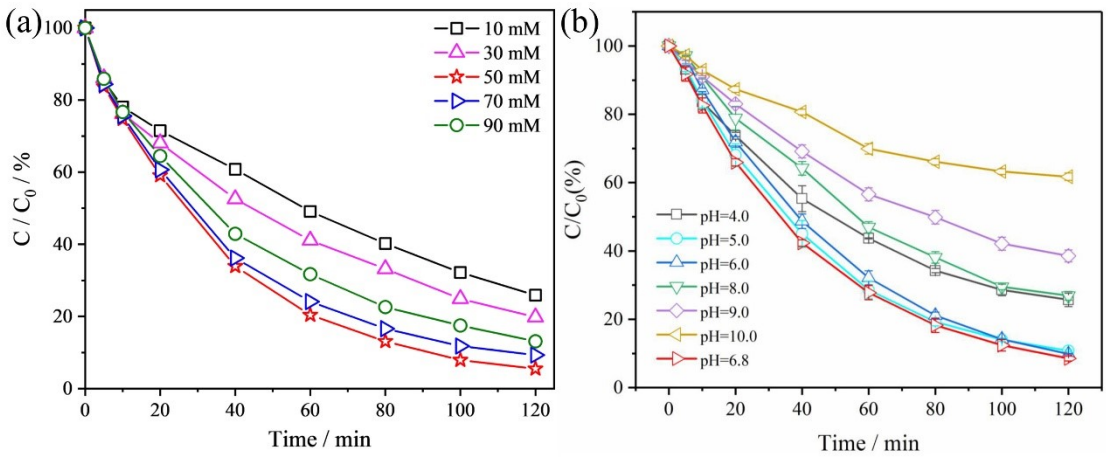

Figure S7. The influence of Na_2SO_4 concentration (a) and pH (b) on the degradation of 2,4-DCP. Reaction condition: applied potential -0.85 V, 2,4-DCP concentration 50 mg/L.

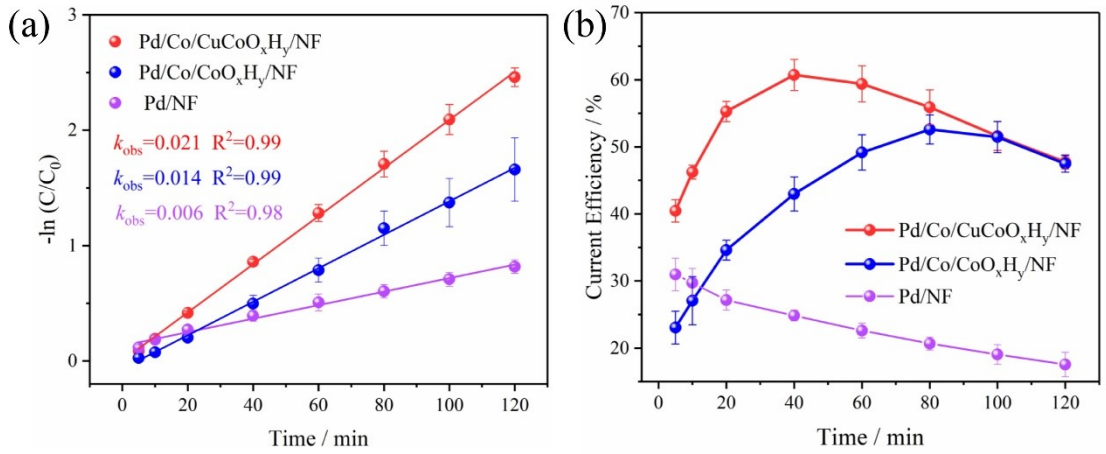

Figure S8. (a) Pseudo-first-order reaction kinetics fitting with different electrodes; (b) current efficiencies at different time intervals recorded on different electrodes.

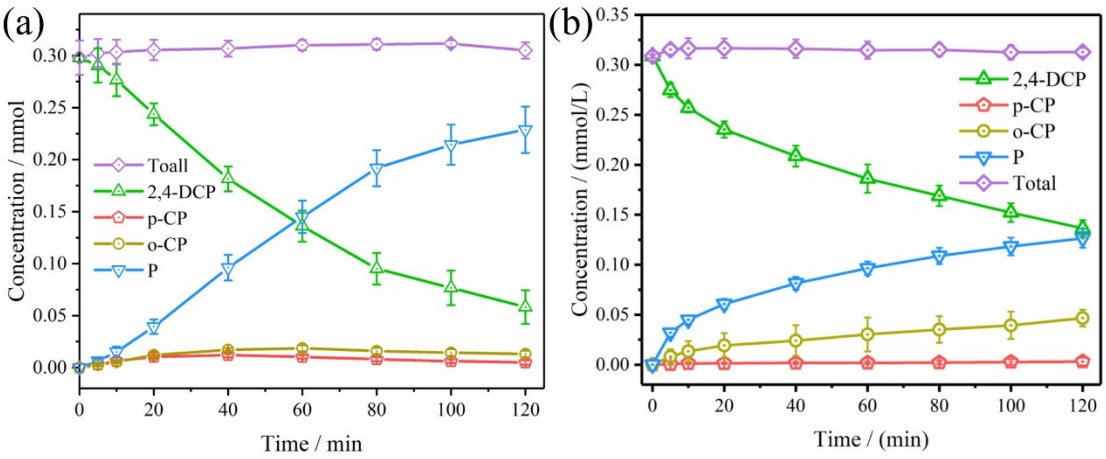

Figure S9. Time-dependent evolution of 2, 4-DCP concentration, o-CP concentration, p-CP concentration, phenol concentration and carbon balance on Pd/Co/CoO_xH_y/NF (a) and Pd/NF (b).

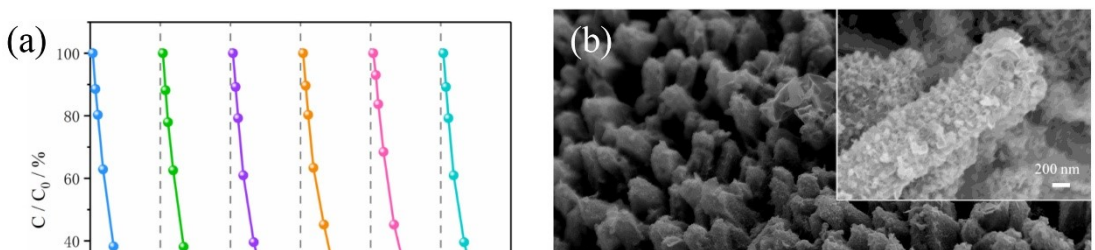

Figure S10. (a) Removal curves of ten consecutive ERD reactions catalyzed by $Pd/Co/CuCoO_xH_y/NF$ at an operation potential of -0.85 V. (b) SEM images of $Pd/Co/CuCoO_xH_y/NF$ after stability test.

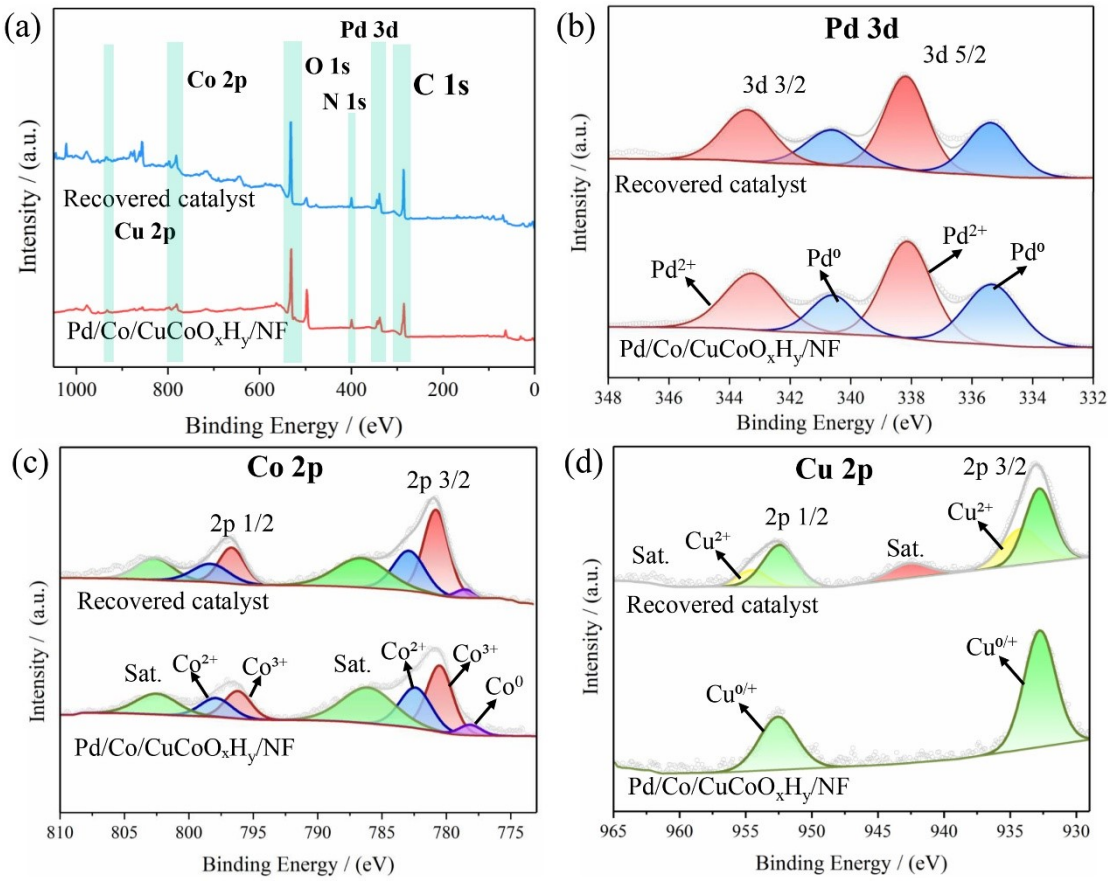

Figure S11, Comparison of XPS spectra of the fresh Pd/Co/CuCoO$_x$H$_y$/NF and the recovered catalyst after stability test: Survey XPS spectra (a), high-resolution Pd 3d XPS spectra (b), high-resolution Co 2p XPS spectra (c), and high-resolution Cu 2p XPS spectra (d).

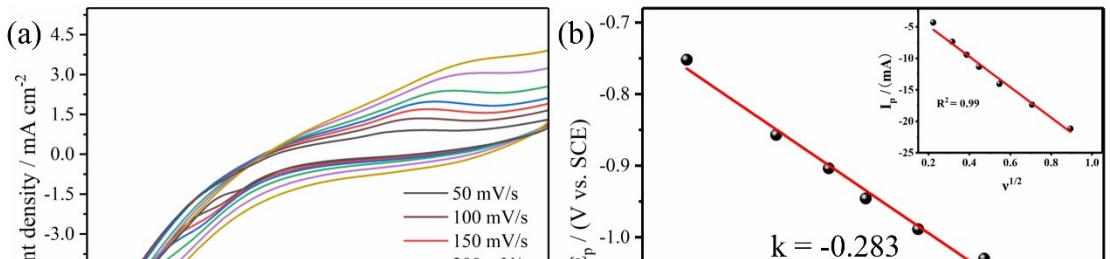

Figure S12. (a) CV curves recorded at scan rates (v) from 50 to 800 mV/s with Pd/Co/$CuCoO_xH_y$/NF as the cathode; reaction condition: 2 mM 2,4-DCP, 50 mM Na_2SO_4. (b) Variation of peak potential as a function of log(v) (inset is the relationship of reduction peak current with the squire root of scan rate).

Note S1.

The ERD reaction mechanism comprises two primary pathways: the indirect electron transfer

(IET) mechanism and the direct electron transfer (DET) mechanism. IET refers to the dechlorination process facilitated by active H* generated on the catalyst surface. The mechanism of the IET route has been summarized in Eqs. (1) - (6) [1]. M represents the metallic surface, while R-Cl denotes chlorinated organic pollutants. The ERD process is essentially a combination of Eqs. (1) - (4), whereas the HER, described by Eqs. (5) and (6), occurs as a competitive process.

$$2H_2O + 2e^- + 2M \rightarrow 2(H)_{ads}M + 2OH^- \ (Volmer\ step) \quad (1)$$

$$R - Cl + M \rightarrow (R - Cl)_{ads}M \quad (2)$$

$$(R - Cl)_{ads}M + 2(H)_{ads}M \rightarrow (R - H)_{ads}M + 2M + HCl \quad (3)$$

$$(R - H)_{ads}M \rightarrow R - H + M \quad (4)$$

$$(H)_{ads}M + H_2O + e^- \rightarrow H_2 + OH^- + M \ (Heyrovsky\ step) \quad (5)$$

$$(H)_{ads}M + (H)_{ads}M \rightarrow H_2 + 2M \ (Tefel\ step) \quad (6)$$

It is well-established that the dechlorination of organic compounds via direct electroreduction can follow two distinct DET pathways: a stepwise one, characterized by the formation of a radical anion intermediate (eq. 1 and 2), or a concerted one, which directly produces a radical and an ion (eq. 3). Because the radical R• is more susceptible to reduction than the parent RCl molecule, the net result is a two-electron reduction wave, as depicted in eq. 1–4 [2].

A reliable way to distinguish these two mechanisms is to measure the ERD process by cyclic voltammetry. With the recorded peak potential (Ep) and $E_{p/2}$ at various scan rates (v), an important parameter, the electron transfer coefficient (α), can be calculated according to eq. 5 and eq. 6. In the concerted pathway, α is typically << 0.5. For the stepwise mechanism, α is determined by the rate-limiting step: it approximates the transfer coefficient (α, often ~0.5) if electron transfer (eq. 1) is slow, but approaches 1.0 if C–Cl cleavage (eq. 2) is rate-limiting. In mixed kinetic regimes, α lies between 0.5 and 1.0. This diagnostic utility of α applies to C–Cl bond electroreduction in both aprotic and protic media [3].

$$RCl + e^- \rightleftharpoons RCl^{\bullet -} \quad (1)$$

$$RCl^{\bullet -} \longrightarrow R^{\bullet} + Cl^- \quad (2)$$

$$RCl + e^- \longrightarrow R^{\bullet} + Cl^- \quad (3)$$

$$R^{\bullet} + e^- \longrightarrow R^- \quad (4)$$

$$\frac{\partial E_p}{\partial log v} = -\frac{1.151RT}{\alpha F} \quad (5)$$

$$E_{P/2} = \frac{1.857RT}{\alpha F} \quad (6)$$

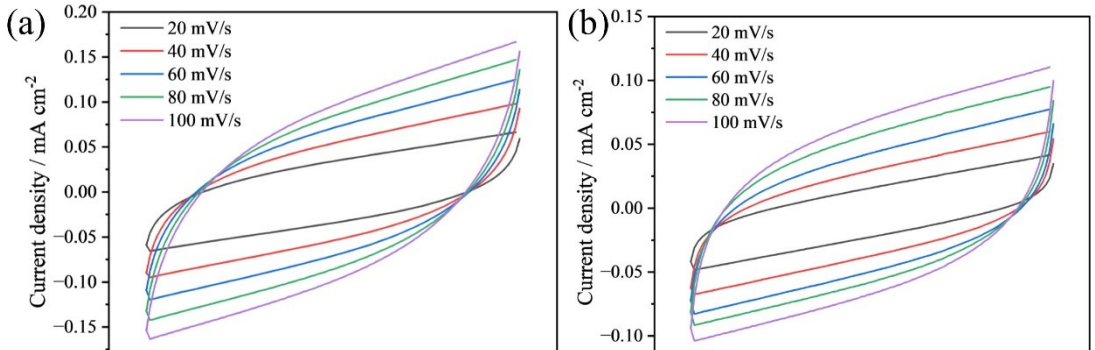

Figure S13. CV curves recorded on Pd/Co/$CuCoO_xH_y$/NF (a) and Pd/Co/CoO_xH_y/NF (b) at various scan rates from 20 to 100 mV/s at the none-Faradic potential region.

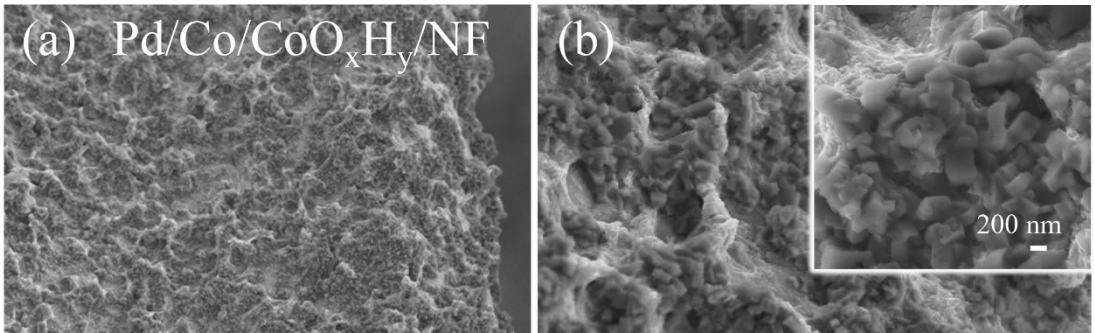

Figure S14. SEM images of Pd/Co/CoO_xH_y/NF with low (a) and high (b) magnifications.

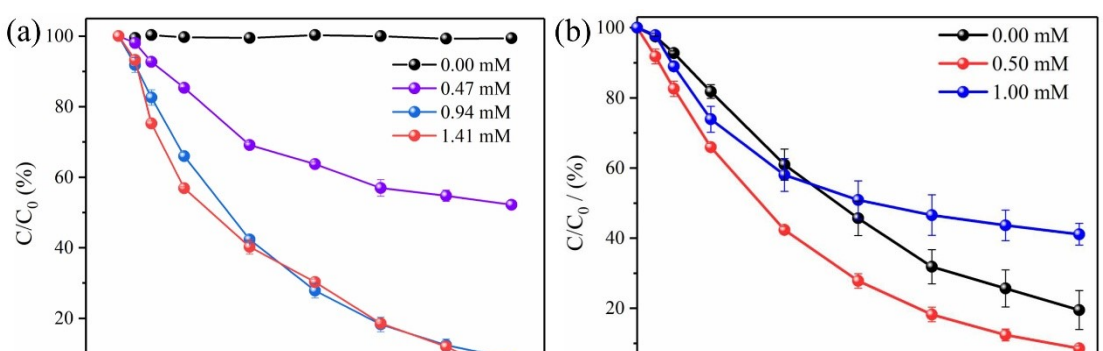

Figure S15. Degradation curves recorded on Pd/Co/$CuCoO_xH_y$/NF electrodes that were prepared with the addition of different concentration of $PdCl_2$ (a) and $Cu(NO_3)_2$ (b).

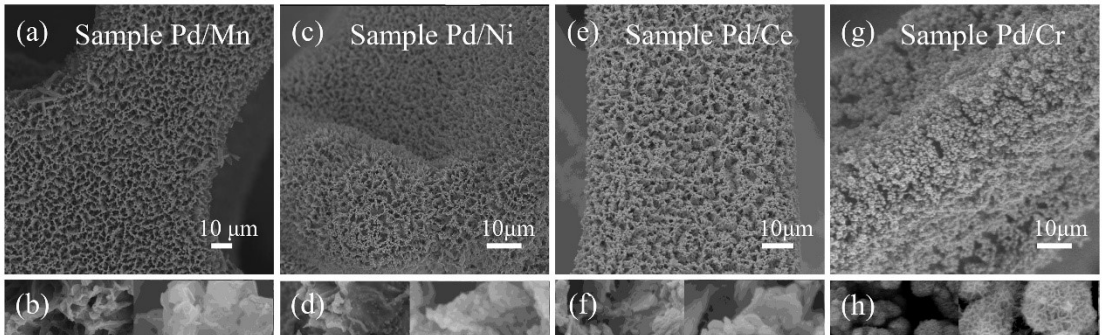

Figure S16. SEM images of Pd/Mn (a, b), Pd/Ni (c, d), Pd/Ce (e, f) and Pd/Cr-based (g, h) hybrid catalyst.

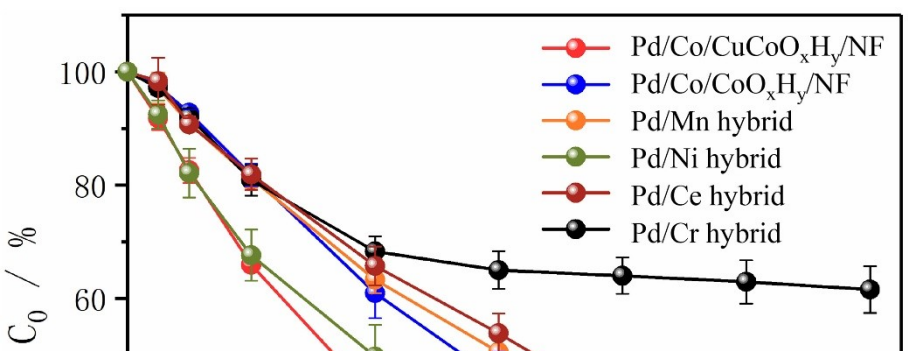

Figure S17. Degradation curves of Pd/Mn-based, Pd/Ni-based, Pd/Ce-based, Pd/Cr-based hybrid Pd/Co/CoO_xH_y/NF and Pd/Co/$CuCoO_xH_y$/NF.

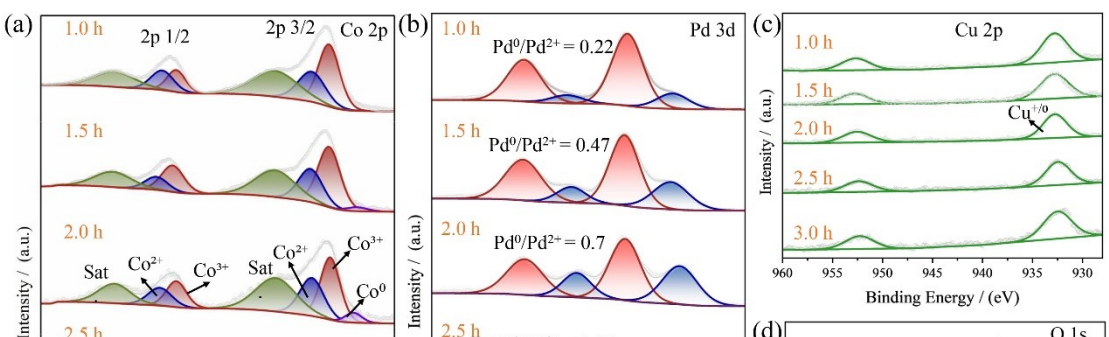

Figure S18. High-resolution Co 2p (a), Pd 3d (b), Cu 2p (c) and O 1s (d) XPS spectra of Pd/Co/$CuCoO_xH_y$/NF prepared by solvothermal reduction of $PdCuCoO_xH_y$ precursor at different time from 1.0 to 3.0 hours.

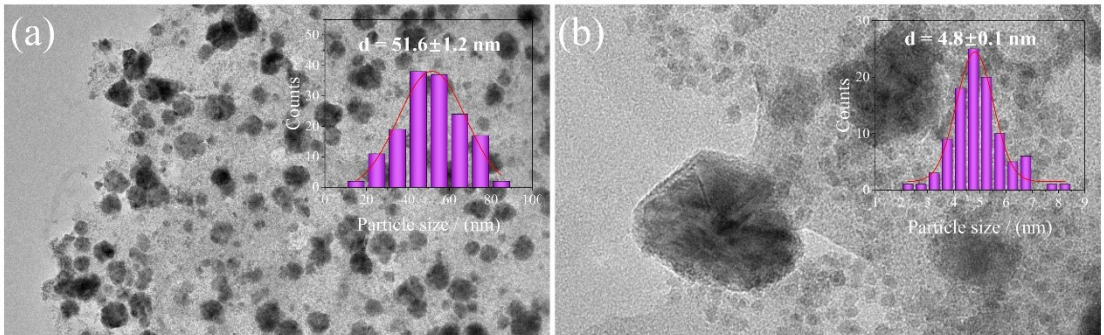

Figure S19. TEM images of Pd/Co/$CuCoO_xH_y$/NF prepared by solvothermal reduction of $PdCuCoO_xH_y$ precursor for 3.0 h. Inset of (a) shows the particle size distribution of Co. Inset of (b) shows the particle size distribution of Pd.

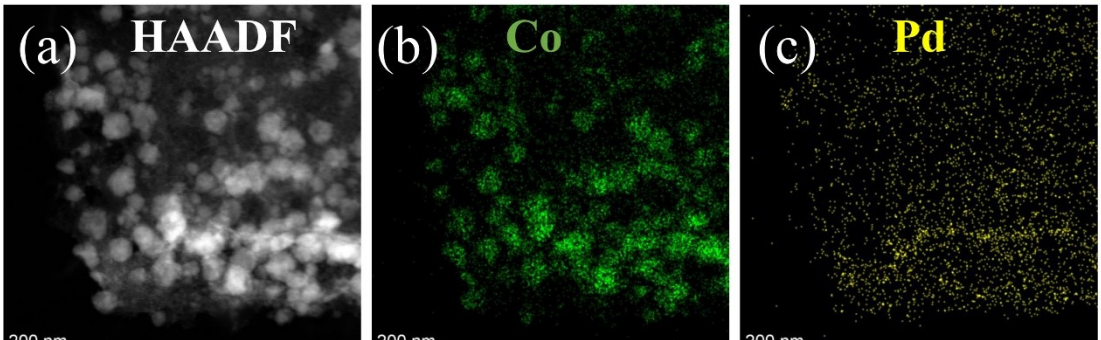

Figure S20. (a) High-angle annular dark-field scanning transmission electron microscopy (HAADF-STEM) image and the corresponding elemental mapping images of (b) Co, (c) Pd, (d) Cu and (e) O.

Table S1. Comparison of EHDC performance between $Pd/Co/CuCoO_xH_y/NF$ and reported in the literature

Cathode materials	Operating conditions	K_{obs} (min^{-1})	Mass activity	Current efficiency	Removal rate	Ref
Pd/C-PEG25	2,4-DCP(0.31mM) Na_2SO_4 (50mM) -0.70V vs.Ag/AgCl	**0.43×10^{-2}**	2.19 ($min^{-1}g^{-1}$)	11.7%	-	[4]
Pd/N-TiO_2/Ti	2,4-DCP (0.61mM) Na_2SO_4 (50mM) -1.24V vs.Hg/Hg_2SO_4	**0.81×10^{-2}**	-	20.08%	84.09% (240 min)	[5]
Pd/TiN	2,4-DCP (0.31mM) Na_2SO_4 (50mM) -0.8V vs.Ag/AgCl (3M)	**1.46×10^{-2}**	4.56 ($min^{-1}g^{-1}$)	~40%	96.4% (240 min)	[6]
Pd/Ni1Co_2-LDH/NF-180	TCAA (0.006mM) Na_2SO_4 (2mM) -0.9V vs.Ag/AgCl (3M)	**1.64×10^{-2}**	32.8 ($min^{-1}g^{-1}$)	~30%	94.81% (180 min)	[7]
Pd-Mn/NF	2,4-DCP (0.31mM) Na_2SO_4 (50mM) -0.85V vs.Ag/AgCl	**3.57×10^{-2}**	9.59 ($min^{-1}g^{-1}$)	29.11%	100% (240 min)	[8]
Pd/MnO_2-Ni foam	2,4-DCP (0.31mM) Na_2SO_4 (50mM) -0.85V vs.Ag/AgCl	**0.883**	0.883 ($min^{-1}mmol^{-1}_{Pd}$)	~24%	100% (150 min)	[9]
Pd/NCMK3-200	2,4-DCP (0.5mM) Na_2SO_4 (10mM) -1.1V vs.SCE	**1.35×10^{-2}**	3.37 ($min^{-1}g^{-1}$)	/	~80% (120 min)	[10]
Pd/U-TiO2	2,4-DCP (0.31mM) Na_2SO_4 (50 mM) -0.85V vs.Ag/AgCl	**9.4×10^{-3}**	4.2 ($min^{-1}g^{-1}$)	21.3%	81.0% (180 min)	[11]
Pd/YS-TiN	2,4-DCP (0.31mM) Na_2SO_4 (50mM) -0.85V vs.Ag/AgCl	**1.43×10^{-2}**	6.06 ($min^{-1}g^{-1}$)	~34%	91.8% (240 min)	[12]
Pd-H_xWO_3/GF	2,4-DCP(0.0613mM) -0.60V vs. SCE	**5.697×10^{-2}**	10.27 ($min^{-1}g^{-1}$)	-	100% (60 min)	[13]

Continued Table S1.

Cathode materials	Operating conditions	K_{obs} (min^{-1})	Mass activity	Current efficiency	Removal rate	Ref
Pd/N-Gr/NF	2,4-DCP (0.62mM) Na_2SO_4 (50mM) I = 6 mA	**6.27×10^{-2}**	-	-	98.6 % (60 min)	[14]
$RuPd_2$	2-CP (0.5 mM) Na_2SO_4 (50mM) -0.85 V vs.Ag/AgCl	**1.02×10^{-2}**	28.3 ($min^{-1}g^{-1}$)	20.8%	97.1% (360min)	[15]
Pd-PdO/MLG	4-CP (1.16 mM) 0.1 M PBS -0.24 V vs. RHE	**7.7×10^{-2}**	634 ($min^{-1}g^{-1}$)	17.4%	88.13% (60 min)	[16]
Pd/Co/$CuCoO_xH_y$/NF	**2,4-DCP (0.31mM)** **Na_2SO_4 (50mM)** **-0.85V vs.SCE**	**2.1×10^{-2}**	**29.17** ($min^{-1}g^{-1}$)	**60.7%**	**91.5%** **(120min)**	**This work**

Table S2. EIS fitting results

Catalyst	R_s (Ω)[a]	R_{ct} (Ω)[b]	R_f (Ω)[c]
Pd/Co/$Co(OH)_x$/NF	4.7	51.79	17.4
PdCu/Co/$Co(OH)_x$/NF	4.7	17.44	46.73

[a]R_s: the resistance of the bulk electrolyte solution; [b]R_{ct}: the charge-transfer resistance for reaction at the interface between the electrode materials and the pore fluids; [C]R_f: the resistance of fluid in the pore space.

Reference:

[1] Xinran Ma, et al. “Recent advances on electrocatalytic hydrodechlorination of chlorinated organic pollutants” Surfaces and Interfaces 75 (2025) 107800

[2]Abdirisak A. Isse, et. al,” Dissociative electron transfer to organic chlorides: Electrocatalysis at metal cathodes” Phys.Chem.Chem.Phys., 2008, 10, 2409–2416

[3] S. Qin, C. Lei, X. Wang, et al., “Electrocatalytic activation of organic chlorides via direct and indirect electron transfer using atomic vacancy control of palladium-based catalyst” Cell Reports Physical Science, 2022, 3, 100713.

[4] Fan, Zhimin, et al. "Enhancing electrocatalytic hydrodechlorination through interfacial microenvironment modulation." Environmental Science & Technology 57.3 (2023): 1499-1509.

[5] Wei, Xuefeng, et al. "Enhanced performance of an in-situ synthesized Pd/N-TiO2/Ti cathode for electrocatalytic hydrodechlorination." Colloids and Surfaces A: Physicochemical and Engineering Aspects 648 (2022): 129320.

[6] Fu, Wenyang, et al. "Identifying the rate-determining step of the electrocatalytic hydrodechlorination reaction on palladium nanoparticles." Nanoscale 11.34 (2019): 15892-15899.

[7] Wang, Jingmin, et al. "Insights into the enhanced performance of NiCo-LDH modified Pd/NF cathode for electrocatalytic hydrodechlorination." Fuel 341 (2023): 127689.

[8] Li, Junxi, et al. "Support electron inductive effect of Pd-Mn/Ni foam catalyst for robust electrocatalytic hydrodechlorination." Journal of Environmental Sciences 149 (2025): 288-300.

[9] Li, Junxi, et al. "Hierarchical Pd/MnO2 nanosheet array supported on Ni foam: an advanced electrode for electrocatalytic hydrodechlorination reaction." Applied Surface Science 509 (2020): 145369.

[10] T. Wu, Y. Zuo, et al., “Electrocatalytic hydrodechlorination of 2,4-dichlorophenol on Pd catalysts supported on N-doped mesoporous carbons: Impact of electronic effects” Applied. Catalysis. A: General, 2023, 666, 119407.

[11] J. Zhang, S. Liu, et al. “Enhanced atomic H* utilization on urchin-like TiO2-supported palladium nanoparticles for efficient electrocatalytic detoxification of chlorinated organics”, Fuel, 2024, 364, 131001.

[12] Zhang, Jun, et al. "Reactant enrichment in yolk-shell structured Pd/TiN nanoreactors for boosting electrocatalytic hydrodechlorination performance." Chemical Engineering Journal 481 (2024): 148325.

[13] Guoshuai Liu, et al. “Electrocatalytic hydrodechlorination of chlorophenols enhanced by hydrogen spillover on Pd-HxWO3 catalysts” Applied Catalysis B: Environment and Energy 384 (2026) 126220

[14] Patrick Rugira, et al. “Experimental and theoretical insights into active hydrogen species on

aconstructed Pd/N-Gr/NF electrode for electrocatalytic hydrodechlorination" Separation and Purification Technology 361 (2025) 131573

[15] Hehe Qian, et al. "Synergistic Surface Engineering of RuPd Nanocatalysts: Orchestrating Reactive Hydrogen Formation, and 2-Chlorophenol Adsorption Dynamics for Enhanced Electrocatalytic Hydrodechlorination" Acs Es&t Engineering. 2025, 5, 3276−3287

[16] Yu Wang, et al. "Efficient Electrocatalytic Hydrodechlorination and Detoxification of Chlorophenols by Palladium−Palladium Oxide Heterostructure" Environmental Science & Technology 2024, 58, 20739−20750